



ELSEVIER

Journal of Alloys and Compounds 291 (1999) 44–51

Journal of
ALLOYS
AND COMPOUNDS

Magnetic structure and properties of $\text{Pb}_8\text{Fe}^{\text{II}}\text{Fe}_2^{\text{III}}\text{F}_{24}$: a 1-D ferrimagnetic chain compound exhibiting a spin-flop transition

A. Pierrard^a, P. Gredin^{a,*}, N. Dupont^a, A. de Kozak^a, F. Bouree-Vigneron^b, G. Andre^b,
I. Rosenman^c

^aLaboratoire de Cristalochimie du Solide, Université Pierre-et-Marie-Curie, 4, place Jussieu, 75252 Paris Cedex 05, France

^bLaboratoire Léon Brillouin, C.E.A.-Saclay, 91191, Gif-sur-Yvette Cedex, France

^cGroupe de Physique des Solides, U.M.R. 7588, 2, place Jussieu, 75251 Paris Cedex 05, France

Received 24 May 1999; accepted 21 June 1999

Abstract

The magnetic structure of $\text{Pb}_8\text{Fe}^{\text{II}}\text{Fe}_2^{\text{III}}\text{F}_{24}$ was solved starting from its neutron diffraction powder pattern obtained at 1.4 K and its magnetic properties were characterized using the data recorded on a SQUID magnetometer and on a magneto-susceptometer. $\text{Pb}_8\text{Fe}^{\text{II}}\text{Fe}_2^{\text{III}}\text{F}_{24}$ is triclinic, space group $P\bar{1}$; its crystal structure was previously solved on a single crystal. The magnetic structure of this fluoride is built up from ferrimagnetic chains antiferromagnetically coupled approximately along the *c*-axis of the cell, making up layers parallel to the (*b*,*c*) plane. Two successive layers exhibit different orientations of the magnetic moments. The net magnetic moment of $\text{Pb}_8\text{Fe}^{\text{II}}\text{Fe}_2^{\text{III}}\text{F}_{24}$ is equal to zero in agreement with an antiferromagnetic structure. This magnetic structure does not evolve in the temperature range: 1.4–20 K. Thus, only one magnetic phase occurs below $T < T_N \approx 21$ K. Under a sufficiently strong magnetic field ($H > 5000$ Oe), $\text{Pb}_8\text{Fe}^{\text{II}}\text{Fe}_2^{\text{III}}\text{F}_{24}$ exhibits a spin-flop transition. © 1999 Published by Elsevier Science S.A. All rights reserved.

Keywords: Iron lead fluoride; Magnetic properties; Neutron diffraction; Magnetic structure; Spin flop transition

1. Introduction

The magnetic properties of one-dimensional compounds were abundantly studied these last years. In particular, theoretical works have focused attention on linear chains in order to estimate various thermodynamic quantities, such as correlation functions, magnetic susceptibility or specific heat. Some authors have investigated the magnetic behaviour of linear ferrimagnetic 1-D systems in which two magnetic cations occupy two or three crystallographic sites [1–6]. Bimetallic chains of connected lozenges were also studied from a theoretical point of view [7]. This kind of ferrimagnetic chain was evidenced in $\text{Ba}_2\text{CaMnFe}_2\text{F}_{14}$ [8] and also in $\text{Pb}_8\text{Fe}^{\text{II}}\text{Fe}_2^{\text{III}}\text{F}_{24}$ [9,10]. The aim of this work is to solve the magnetic structure of this latter fluoride and to specify its magnetic properties in relation with its crystal and magnetic structures.

2. Experimental

The binary fluorides used in this work were prepared in the laboratory.

To obtain iron III fluoride, first $\text{FeF}_3 \cdot 3\text{H}_2\text{O}$ is prepared in solution by reaction in a platinum crucible between $\text{Fe}(\text{NO}_3)_3 \cdot 9\text{H}_2\text{O}$ (R.P. Normapur) and an excess of hydrofluoric acid at 40% (R.P. Normapur); the liquid is evaporated on a sand-bath at 60°C and the solid is then slowly dehydrated in 6 h into FeF_3 under an anhydrous hydrogen fluoride stream at 750°C.

Iron II fluoride is prepared starting from $\text{FeCl}_2 \cdot 4\text{H}_2\text{O}$ (R.P. Normapur). The chloride is first dehydrated into FeCl_2 under an anhydrous hydrogen chloride stream at 250°C in 3 h and then immediately fluorinated in the same reactor into FeF_2 by anhydrous hydrogen fluoride at 650°C in 4 h.

Lead fluoride PbF_2 is synthesized in solution by reaction between its carbonate (R.P. Rectapur) and an excess of hydrofluoric acid at 40% (R.P. Normapur); the liquid is evaporated at 80°C and the solid is then dried in 4 h at 500°C under argon.

$\text{Pb}_8\text{Fe}^{\text{II}}\text{Fe}_2^{\text{III}}\text{F}_{24}$ is prepared by reaction in the solid state

*Corresponding author.

E-mail address: gredin@ccr.jussieu.fr (P. Gredin)

of a stoichiometric mixture of the three fluorides PbF_2 , FeF_2 and FeF_3 placed in a platinum crucible under dried argon, at 500°C during 14 h.

The neutron diffraction experiments were performed at the Laboratoire Léon Brillouin (C. E. A. Saclay) using the 3T2 and G4.1 diffractometers. The high resolution powder diffractometer 3T2 ($\lambda=1.2253 \text{ \AA}$, $6^\circ < 2\theta < 126^\circ$) was used for the refinement of the nuclear structure at 300 K and the multi-detector (800 cells) G4.1 ($\lambda=2.4266 \text{ \AA}$) was used for the resolution of the magnetic structure and the thermal evolution study of the low temperature diagrams. Therefore, twelve diffraction patterns were recorded in the range $2\theta=7\text{--}87^\circ$, at different temperatures between 43 and 1.4 K. The powder sample was put in a cylindrical vanadium can and held in a liquid helium cryostat. Nuclear and magnetic structures were refined using the program FULLPROF [11]. The nuclear scattering lengths and magnetic forms were those included in this program.

The magnetic susceptibility was determined between 300 and 2 K using a SQUID magnetometer. The data were corrected from the diamagnetism of the sample, using the usual values for Fe^{2+} , Fe^{3+} , Pb^{2+} and F^- ions [12]. The field dependence of the magnetization at 5 K was obtained between 0 and 15,000 Oe using a DSM8 MANICS magneto-susceptometer.

3. Structural background

$\text{Pb}_8\text{Fe}^{\text{II}}\text{Fe}_2^{\text{III}}\text{F}_{24}$ is triclinic with the cell parameters determined from X-ray diffraction: $a=20.118(3) \text{ \AA}$, $b=$

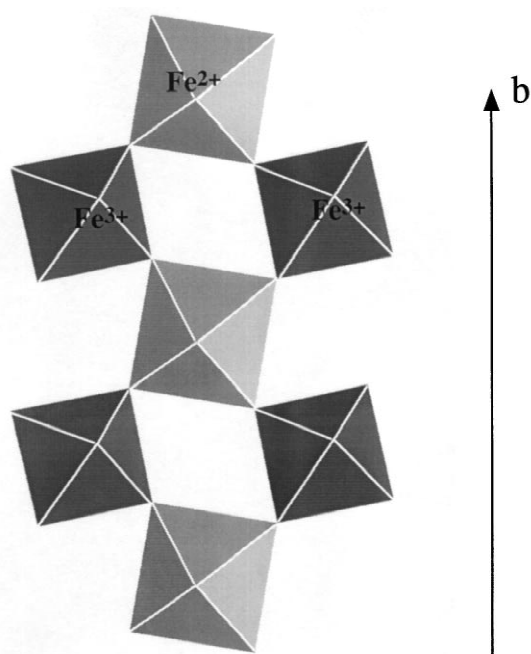


Fig. 1. (1 0 0) projection of the infinite $[\text{Fe}^{\text{II}}\text{Fe}^{\text{III}}\text{F}_{14}]_n^{6n-}$ double-chains, running along the b -axis.

$5.597(1) \text{ \AA}$, $c=9.440(2) \text{ \AA}$, $\alpha=89.75(2)^\circ$, $\beta=105.79(2)^\circ$, $\gamma=89.38(2)^\circ$, $Z=2$. The crystal structure was previously solved in the unconventional space group $C\bar{1}$ from X-ray single crystal data [10]. The cationic subnetwork of $\text{Pb}_8\text{Fe}^{\text{II}}\text{Fe}_2^{\text{III}}\text{F}_{24}$ is quite the same that the one observed for the fluorite-type structure adopted by PbF_2 at high temperature. The compound is obtained by a strict ordered substitution of 3/11th of the lead cations of PbF_2 by iron cations, which adopt, as usual in fluorides, an octahedral coordination. The iron III octahedron is quite regular, with a mean $\text{Fe(III)}\text{--F}$ distance of 1.924 \AA . The iron II octahedron is distorted by a compressive Jahn–Teller effect, in agreement with a d^6 HS electronic configuration. The iron octahedra share corners and form infinite $[\text{Fe}^{\text{II}}\text{Fe}^{\text{III}}\text{F}_{14}]_n^{6n-}$ double-chains (Fig. 1) running along the b -axis, inserted in a fluorite-like matrix (Fig. 2). The crystal structure of $\text{Pb}_8\text{FeFe}_2\text{F}_{24}$ and related compounds, must be compared to that of the mineral called ‘usovite’: $\text{Ba}_2\text{CaMgAl}_2\text{F}_{14}$ [8], which exhibits the same $[\text{M}^{\text{II}}\text{M}^{\text{III}}\text{F}_{14}]_n^{6n-}$ double-chains and has therefore about the same b cell parameter.

4. Nuclear and magnetic structure determinations

The neutron powder diffraction pattern obtained on the 3T2 diffractometer at 300 K was refined starting from the atomic positions determined from the X-ray single crystal data [10]. After refinement of the cell parameters, zero-point, atomic positions and isotropic thermal motions, the reliability factors converge to rather good values, taking into account the number of refined parameters and the complexity of the powder pattern. The characteristics of the refinement are given in Table 1 and the observed and calculated diffraction diagrams are shown in Fig. 3.

The atomic positions determined from the neutron powder pattern at 300 K are given in Table 2. These are very close to those obtained from the X-ray diffraction data [10]. Considering the accuracy of the measurements and the complexity of the neutron diffraction pattern, the two techniques lead to the same close atomic positions. The values of the isotropic thermal factors are high, but in the range of those obtained for other compounds [13–15]. Moreover, these values exhibit the same unusual order as observed from X-ray diffraction, i.e., $B_{\text{eq.}}(\text{Pb})$ greater than $B_{\text{eq.}}(\text{Fe})$. The η factor exhibits a high value which indicates a line broadening. This effect can be attributed to the relatively poor crystallinity of the powder. Indeed, in this case, the line broadening results from the finite extent of the coherently diffracting domains within the grains.

To solve the magnetic structure of $\text{Pb}_8\text{Fe}^{\text{II}}\text{Fe}_2^{\text{III}}\text{F}_{24}$, twelve neutron diffraction patterns were recorded on the G4.1 diffractometer between 43 and 1.4 K. These patterns do not allow to refine the atomic positions. Indeed, the ratio between the number of effective reflections and the number of intensity dependent parameters is too low.

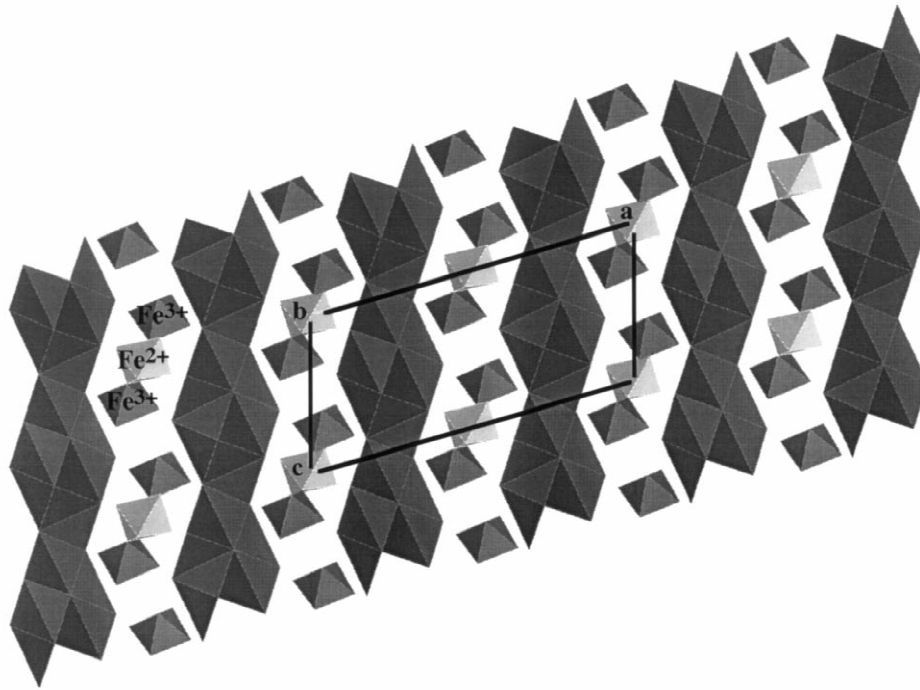


Fig. 2. (0 1 0) projection of the structure of $\text{Pb}_8\text{Fe}^{\text{II}}\text{Fe}_2^{\text{III}}\text{F}_{24}$ showing a sort of layered structure separating fluorite-type zones from perovskite-type ones.

Therefore the atomic positions found at 300 K were used in the refinement of the patterns and only the cell parameters, the values and the directions of the magnetic moments were refined. Above 21 K, no magnetic lines are observed. Below 21 K, the order temperature, new lines, the strongest ones of which lie in the 2θ range: $6\text{--}55^\circ$, appear and are attributed to the magnetic structure (Fig. 4). They can be indexed in a double cell, with the parameters: $a_{\text{magnetic}} = a_{\text{nuclear}}$, $b_{\text{magnetic}} = b_{\text{nuclear}}$, $c_{\text{magnetic}} = 2c_{\text{nuclear}}$, $\alpha_{\text{magnetic}} = \alpha_{\text{nuclear}}$, $\beta_{\text{magnetic}} = \beta_{\text{nuclear}}$ and $\gamma_{\text{magnetic}} = \gamma_{\text{nuclear}}$.

As the nuclear structure belongs to the triclinic unconventional space group $C\bar{1}$, the magnetic structure will be solved in the lower symmetry space group $P1$, using the neutron diffraction pattern obtained at 1.4 K. It can be noted that large diffusion peaks are observed above the Néel temperature around $2\theta = 8^\circ$ and $2\theta = 28^\circ$ (see neutron diffraction pattern obtained at 24 K in Fig. 4). This indicates that a short range ordering of the magnetic moments occurs. The diffusion still subsists below the Néel temperature, even at 1.4 K, particularly around $2\theta = 8^\circ$,

Table 1
Crystallographic data and refinement characteristics (nuclear cell)

System and space group (nuclear structure)	Triclinic $C\bar{1}$ ($P\bar{1}$)
Refined cell parameters: $a = 20.133(4) \text{ \AA}$, $b = 5.6006(1) \text{ \AA}$, $c = 9.4344(2) \text{ \AA}$, $\alpha = 89.625(2)^\circ$, $\beta = 105.583(2)^\circ$, $\gamma = 89.509(2)^\circ$, $Z = 2$	
Wavelength	1.2253 \AA
2θ data range and step	$6\text{--}126^\circ \times 0.05^\circ$
Number of independent reflections	3278
Effective number of reflections taken into account for the resolution	342
Number of intensity dependent parameters	54
Halfwidth parameters ($H^2 = U \cdot \tan^2 \theta + V \cdot \tan \theta + W$)	
U:	0.3225
V:	-0.4975
W:	0.2475
η (pseudo-Voigt profile)	0.30(1)
Rietveld reliability factors (%)	
R_p :	8.65
R_{wp} :	9.12
R_B :	6.31
R_F :	4.26

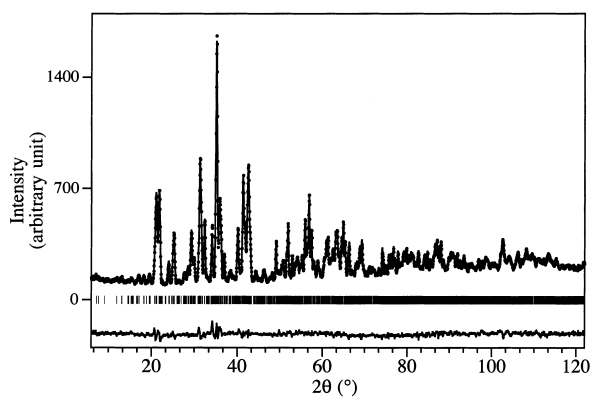


Fig. 3. Observed (dotted line) and calculated (solid line) profiles of the neutron powder pattern of $\text{Pb}_8\text{Fe}^{\text{II}}\text{Fe}_2^{\text{III}}\text{F}_{24}$ obtained on the 3T2 diffractometer at 300 K. The short vertical lines below the patterns mark the positions of all Bragg reflections. The bottom curve shows the difference between observed and calculated profiles.

Table 2

Atomic coordinates and parameters of isotropic thermal motion (with e.s.d. in parentheses)

Atom	<i>x</i>	<i>y</i>	<i>z</i>	$B_{\text{eq.}}$ (\AA^2)
Pb(1)	0.7236(14)	0.0063(23)	0.6387(17)	1.10(13)
Pb(2)	0.6317(13)	0.0085(21)	0.1701(17)	1.10(13)
Pb(3)	0.8232(13)	-0.0029(22)	0.1023(17)	1.10(13)
Pb(4)	0.0852(13)	0.0034(22)	0.4383(16)	1.10(13)
Fe(2)	0	0	0	0.32(8)
Fe(3)	0.5460(13)	0.0038(21)	0.7491(16)	0.32(8)
F(1)	0.7241(16)	0.2550(31)	0.1233(21)	1.53(13)
F(2)	0.1787(16)	0.2511(29)	0.3960(21)	1.53(13)
F(3)	0.6835(16)	0.2466(33)	0.3870(21)	1.53(13)
F(4)	0.6415(15)	0.0618(27)	0.8597(20)	1.53(13)
F(5)	0.9562(15)	0.2120(28)	0.3625(20)	1.53(13)
F(6)	0.8227(15)	0.0600(27)	0.3564(20)	1.53(13)
F(7)	0.4469(15)	0.2772(27)	0.1139(20)	1.53(13)
F(8)	0.9786(5)	0.3131(27)	0.0979(20)	1.53(13)
F(9)	0.4128(15)	0.1840(27)	0.3686(20)	1.53(13)
F(10)	0.5475(15)	0.0493(27)	0.3390(19)	1.53(13)
F(11)	0.9097(15)	0.0406(28)	0.8573(20)	1.53(13)
F(12)	0.2283(16)	0.2615(31)	0.1342(21)	1.53(13)

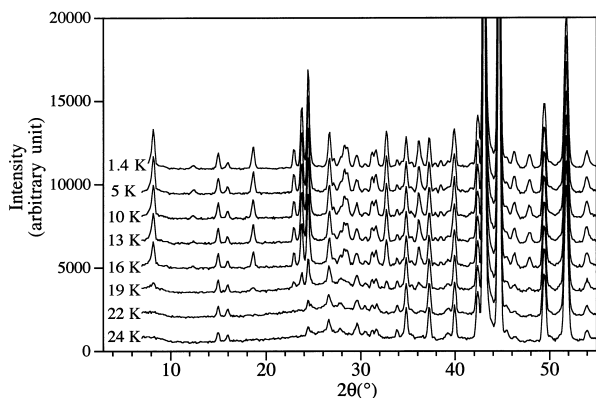


Fig. 4. Thermal evolution of the neutron powder patterns for $\text{Pb}_8\text{Fe}^{\text{II}}\text{Fe}_2^{\text{III}}\text{F}_{24}$ between 24 and 1.4 K showing the increase of the magnetic lines in the 2θ range: $7\text{--}55^\circ$.

under the $0\ 0\ 1$ magnetic diffraction line. Therefore, a weak long range magnetic disorder exists up to 1.4 K. This observation is corroborated by the greater value of the profile shape parameter η for the magnetic phase than for the nuclear one (see Table 3).

Fig. 5 shows the positions of the iron II and III in the magnetic cell. A careful analysis of the zero intensity magnetic lines hkl , with $l = 2n$, implies that magnetic

Table 3

Refinement characteristics for the magnetic structure determination

System and space group (magnetic structure)	Triclinic $P1$
Refined magnetic cell parameters at 1.4 K: $a = 20.046(2)\ \text{\AA}$, $b = 5.621(1)\ \text{\AA}$, $c = 18.781(1)\ \text{\AA}$ $\alpha = \gamma = 90^\circ$, $\beta = 105.43(1)^\circ$, $Z = 4$	
Wavelength	2.4266 \AA
2θ data range and step	$7\text{--}55^\circ \times 0.1^\circ$
Number of independent reflections	284
Effective number of reflections taken into account for the resolution	56
Number of intensity dependent parameters	4
Halfwidth parameters ($H^2 = U \cdot \tan^2 \theta + V \cdot \tan \theta + W$)	
U :	0.821
V :	-0.237
W :	0.078
η (pseudo-Voigt profile) for the nuclear phase	0.50(2)
η (pseudo-Voigt profile) for the magnetic phase	0.71(4)
Rietveld reliability factors (%)	
R_p :	11.1
R_{wp} :	11.4
R_B :	3.67
R_{Magnetic} :	6.63

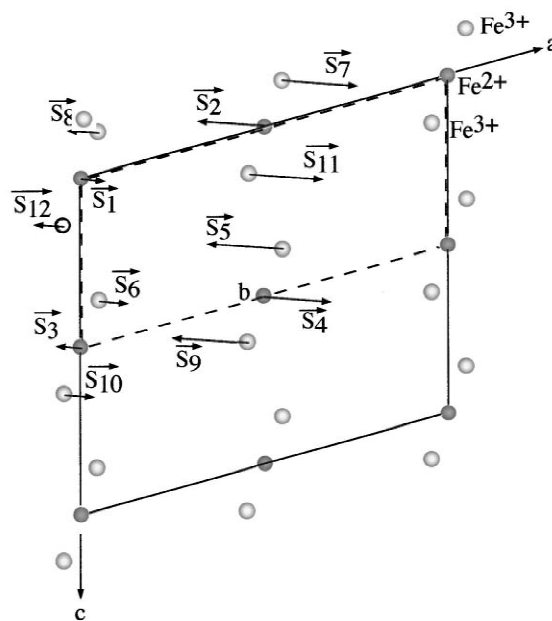


Fig. 5. : $(0\ 1\ 0)$ projection of the structure of $\text{Pb}_8\text{Fe}^{\text{II}}\text{Fe}_2^{\text{III}}\text{F}_{24}$ showing the orientations of the projections of the magnetic moments. The nuclear and the magnetic cells are drawn with hatched lines and solid lines respectively.

moments linked by the \vec{c} translation are opposite to each other i.e.:

$$\vec{S}_1 = -\vec{S}_3; \vec{S}_2 = -\vec{S}_4$$

$$\vec{S}_5 = -\vec{S}_7; \vec{S}_6 = -\vec{S}_8$$

$$\vec{S}_9 = -\vec{S}_{11}; \vec{S}_{10} = -\vec{S}_{12}$$

Assuming that the magnetic moments of iron III in a $[\text{Fe}^{\text{II}}\text{Fe}_2^{\text{III}}\text{F}_{14}]_n^{6n-}$ chain have the same directions and values (i.e.: $\vec{S}_5 = \vec{S}_9$, $\vec{S}_6 = \vec{S}_{10}$, $\vec{S}_7 = \vec{S}_{11}$ and $\vec{S}_8 = \vec{S}_{12}$), all the relations between the magnetic moments allow to find a starting model for the refinement of the magnetic structure. Moreover, the curve of the magnetic susceptibility versus the temperature is characteristic of ferrimagnetic chains and so, we assume that the magnetic moments of iron III exhibit in a same chain an antiferromagnetic coupling with the magnetic moments of iron II. The measurements of the magnetization versus the field show that the net magnetic moment is approximately null for $H=0$, which leads to an antiferromagnetic structure at field $H=0$ and at $T < 21$ K (Fig. 12).

In fact, different possible solutions can be checked. For a first solution (model I), the magnetic moments of iron III exhibit an antiferromagnetic coupling with the magnetic moments of iron II located in the same chain and they are both collinear. For a second one (model II), the magnetic moments of iron III exhibit in a same chain an antiferromagnetic coupling with the magnetic moments of iron II and they can be both non-collinear, i.e. giving an angle slightly different from 180° . The model II compared to the model I, leads to the same reliability factors and at the final stage of the refinements, the θ angles and the magnetic moments appear to be the same, taking into account the standard deviations. Therefore, only model I was retained.

The refinement of the nuclear and magnetic cell parameters shows that the angles α and γ become very close to 90° (respectively $89.95(3)$ and $89.94(5)$) below 20 K. Therefore, the angles α and γ were fixed at 90° for the magnetic cell and a system of spherical coordinates defined in Fig. 6, is used to solve the magnetic structure of $\text{Pb}_8\text{Fe}^{\text{II}}\text{Fe}_2^{\text{III}}\text{F}_{24}$. This choice gives better results than the use of cartesian coordinates, due to the reduction of the number of refinable parameters. The characteristics of the refinement are given in Table 3. The ϕ angle can vary from 0 to 26° , without sensible modifications on the calculated neutron diffraction pattern. Nevertheless, the best reliability factors were obtained for $\phi = 19^\circ$ and so, ϕ is fixed at this value for all the refinements. The values of the magnetic moments and their directions are given in spherical coordinates in Table 4. The difference curve between calculated and experimental powder diffraction patterns is given in Fig. 7.

As described in the structural part, the $[\text{Fe}^{\text{II}}\text{F}_6]^{4-}$ octahedron exhibits a compressive Jahn–Teller effect, in

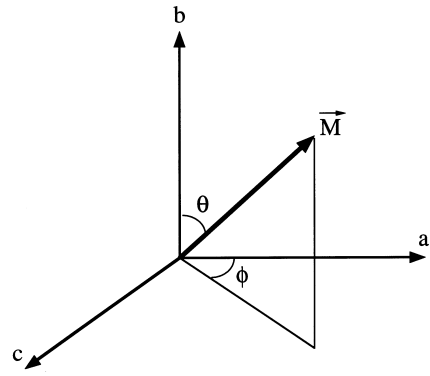


Fig. 6. : Definition of the θ and ϕ angles of the spherical coordinates in relation with the crystallographic axes.

Table 4

Positions of the magnetic atoms, values and directions of the magnetic moments^a

Atom	Label	x	y	z	M (μ_B)	ϕ ($^\circ$)	θ ($^\circ$)
Fe ²⁺	S ₁	0	0	0	3.70(6)	19	165(3)
Fe ²⁺	S ₂	0.5	0.5	0	3.70(6)	19	215(3)
Fe ²⁺	S ₃	0	0	0.5	3.70(6)	19	345(3)
Fe ²⁺	S ₄	0.5	0.5	0.5	3.70(6)	19	35(3)
Fe ³⁺	S ₅	0.5460	0.0038	0.3746	4.38(5)	19	215(3)
Fe ³⁺	S ₆	0.0460	0.5038	0.3746	4.38(5)	19	165(3)
Fe ³⁺	S ₇	0.5460	0.0038	0.8746	4.38(5)	19	35(3)
Fe ³⁺	S ₈	0.0460	0.5038	0.8746	4.38(5)	19	345(3)
Fe ³⁺	S ₉	-0.5460	-0.0038	-0.3746	4.38(5)	19	215(3)
Fe ³⁺	S ₁₀	-0.0460	-0.5038	-0.3746	4.38(5)	19	165(3)
Fe ³⁺	S ₁₁	-0.5460	-0.0038	-0.8746	4.38(5)	19	35(3)
Fe ³⁺	S ₁₂	-0.0460	-0.5038	-0.8746	4.38(5)	19	345(3)

^a The coordinates of the iron ions are given in the magnetic cell: $a_{\text{nuclear}} \times b_{\text{nuclear}} \times 2c_{\text{nuclear}}$.

agreement with a d^6 HS electronic configuration. Indeed, the orbital component of the magnetic moment is close to zero and a 'spin only' magnetic moment is assumed. So,

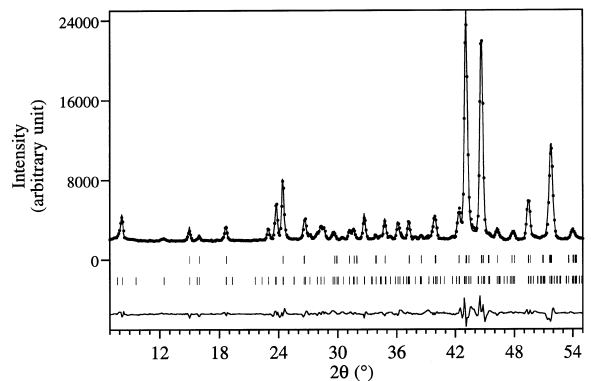


Fig. 7. Observed (dotted line) and calculated (solid line) profiles of the neutron powder pattern of $\text{Pb}_8\text{Fe}^{\text{II}}\text{Fe}_2^{\text{III}}\text{F}_{24}$ obtained on the G4.1 diffractometer at 1.4 K. The short vertical lines below the patterns mark the positions of all Bragg reflections (nuclear and magnetic lines). The bottom curve shows the difference between observed and calculated profiles.

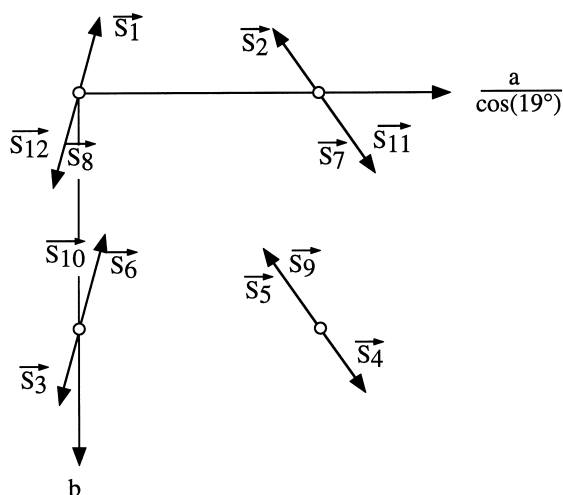


Fig. 8. Orientations of the magnetic moments on the $(a/\cos(19^\circ), b)$ plane.

the magnetic moments of iron II and III (Table 4) correspond approximately to 90% of their theoretical values, 4 and 5 μ_B respectively.

The magnetic structure of $\text{Pb}_8\text{Fe}^{\text{II}}\text{Fe}_2^{\text{III}}\text{F}_{24}$ can be described as built up from successive antiferromagnetic $[\text{Fe}_2^{\text{II}}\text{Fe}_4^{\text{III}}\text{F}_{28}]_n^{12n-}$ layers parallel to the (b,c) plane. Indeed, these layers are composed with ferrimagnetic $[\text{Fe}^{\text{II}}\text{Fe}_2^{\text{III}}\text{F}_{14}]_n^{6n-}$ chains running along the b -axis of the magnetic cell. Two successive ferrimagnetic chains exhibit an antiferromagnetic coupling along the c -axis of the magnetic cell. Then, all the net magnetic moments are compensated. Two successive layers are separated along the a -axis by fluorite-type $[\text{Pb}_{16}\text{F}_{20}]_n^{12n+}$ blocks and exhibit different orientations of their iron II and III magnetic moments (Figs. 5,8).

Fig. 9 gives the evolution of the iron II and III magnetic moments versus the temperature refined with the same magnetic model, giving a Néel temperature around 21 K. The values of the magnetic moments follow a Brillouin

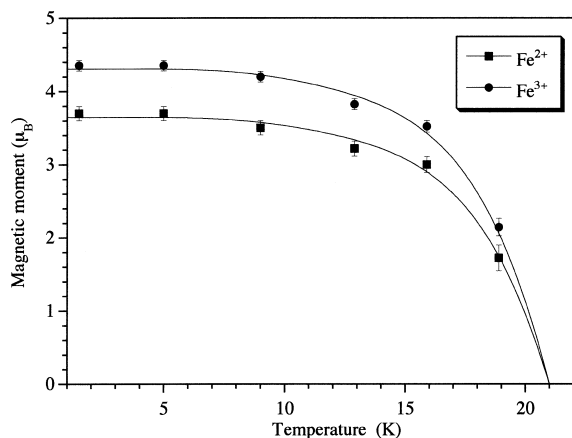


Fig. 9. Evolution of the magnetic moments of iron II and III versus the temperature.

law. They are saturated below 9 K. Nevertheless, as indicated above, the values of the Fe^{2+} and Fe^{3+} magnetic moments are lower than the expected ones for the free ions. This fact can be explained by the presence of the diffusion which still subsists even at 1.4 K.

The magnetic structure of $\text{Pb}_8\text{Fe}^{\text{II}}\text{Fe}_2^{\text{III}}\text{F}_{24}$ can be compared to that of the usovite-type compound $\text{Ba}_2\text{CaMnFe}_2\text{F}_{14}$ in which the same type of ferrimagnetic chains has been evidenced [8]. Nevertheless, on the contrary of $\text{Pb}_8\text{Fe}^{\text{II}}\text{Fe}_2^{\text{III}}\text{F}_{24}$, $\text{Ba}_2\text{CaMnFe}_2\text{F}_{14}$ is built up from ferromagnetic $[\text{CaMnFe}_2\text{F}_{14}]_n^{4n-}$ layers, which are perpendicular to the a -axis. In the a direction, the layers are coupled antiferromagnetically and all the magnetic moments are compensated, leading to an antiferromagnetic compound.

5. Magnetic properties of $\text{Pb}_8\text{Fe}^{\text{II}}\text{Fe}_2^{\text{III}}\text{F}_{24}$

Fig. 10 shows the plot of the reciprocal molar susceptibility χ_M^{-1} versus the temperature, obtained under 1000 and 15,000 Oe magnetic fields. A Curie–Weiss law is well obeyed above 200 K, with $C_M = 11.84 \text{ cm}^3 \cdot \text{K} \cdot \text{mol}^{-1}$ and $\theta_p = -85 \text{ K}$. The observed value for the Curie constant C_M is in agreement with the calculated one for two iron III and one iron II exhibiting ‘spin only’ moments ($11.74 \text{ cm}^3 \cdot \text{K} \cdot \text{mol}^{-1}$). Below 200 K, χ_M^{-1} versus temperature, under a 1000 Oe magnetic field, shows a non-linear decrease until 21 K, the Néel temperature. The plot of χT versus temperature displayed in Fig. 11, exhibits a minimum of χT around 120 K. This magnetic behaviour, characteristic of ferrimagnetic chains, is also observed for $\text{Ba}_2\text{CaMnFe}_2\text{F}_{14}$ [8]. This kind of ferrimagnetic chain was theoretically studied by Xu et al. [7] considering a classical Heisenberg spin Hamiltonian.

The field dependence of the magnetization at 5 K was measured between 0 and 15,000 Oe (Fig. 12). The curve is characteristic of a spin-flop transition which occurs for a

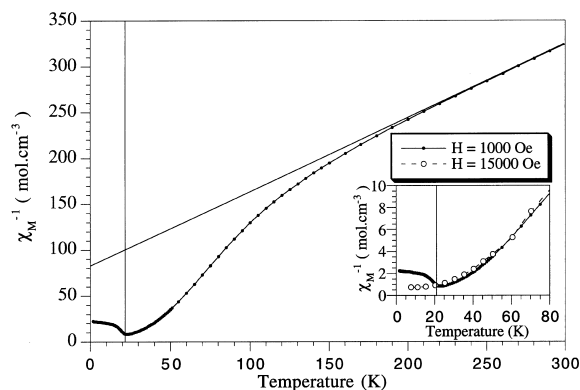


Fig. 10. Plot of the reciprocal molar susceptibility of $\text{Pb}_8\text{Fe}^{\text{II}}\text{Fe}_2^{\text{III}}\text{F}_{24}$ versus the temperature. The insert in the figure shows the plot of the reciprocal molar susceptibility versus the temperature for magnetic fields: $H = 1000 \text{ Oe}$ and $H = 15,000 \text{ Oe}$.

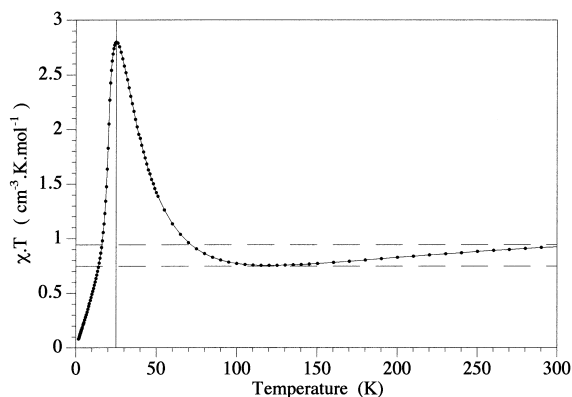


Fig. 11. Plot of χT versus temperature for $\text{Pb}_8\text{Fe}^{\text{II}}\text{Fe}_2^{\text{III}}\text{F}_{24}$.

critical magnetic field around $H_s = 5000$ Oe. Indeed, the magnetization exhibits a weak linear increase from 0 to 5000 Oe. Above 5000 Oe, the magnetization increase becomes non linear and reaches a value of $4.2 \mu_B$ for 15,000 Oe. The magnetization cycle versus the magnetic field shows a weak hysteresis as expected for a spin-flop transition.

To explain this behaviour, in connection with the magnetic structure of $\text{Pb}_8\text{Fe}^{\text{II}}\text{Fe}_2^{\text{III}}\text{F}_{24}$, we propose a transition mechanism. Indeed, the coupling between the magnetic moments of iron II and iron III in a same chain is strong. On the contrary, the coupling between adjacent chains and all the more between the layers, is sufficiently weak for that the magnetic moments of iron II and correlatively iron III, fall into line when the magnetic field increases and becomes sufficiently strong. $\text{Pb}_8\text{Fe}^{\text{II}}\text{Fe}_2^{\text{III}}\text{F}_{24}$ falls over from an antiferromagnetic state to a saturated paramagnetic state, sometimes called ferromagnetic state. Therefore, the value of the net magnetic moment of the compound must reach the one of a $[\text{Fe}^{\text{II}}\text{Fe}_2^{\text{III}}\text{F}_{14}]_n^{6n-}$ chain, i.e. approximately $5 \mu_B$. The measured value at 5 K and under a 15,000 Oe magnetic field is weakly lower than the

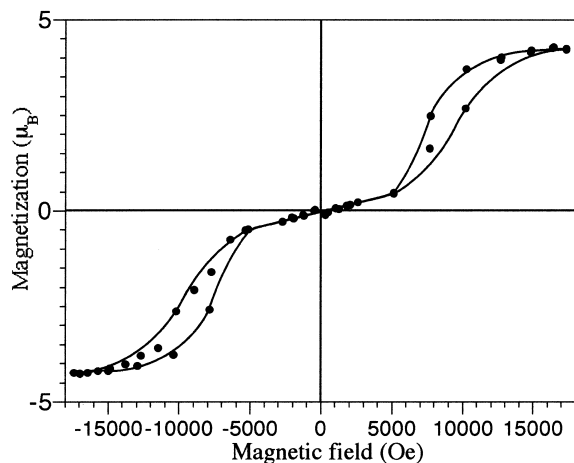


Fig. 12. Plot of the magnetization of $\text{Pb}_8\text{Fe}^{\text{II}}\text{Fe}_2^{\text{III}}\text{F}_{24}$ versus the magnetic field.

calculated one using the magnetic moments issued from the resolution of the magnetic structure, due probably to a residual angle between the magnetic moments. The existence of a spin-flop transition explains the different behaviour observed at low temperature for the plots of the reciprocal molar susceptibility χ_{M}^{-1} versus the temperature, obtained under 15,000 and 1000 Oe magnetic fields. Under a 15,000 Oe magnetic field, the compound is ferrimagnetic and the plot χ_{M}^{-1} versus the temperature is characteristic of a 1-D ferrimagnetic lozenges chain $[\text{Fe}^{\text{II}}\text{Fe}_2^{\text{III}}\text{F}_{14}]_n^{6n-}$ [7,8].

Because of all the measurements were carried on powdered samples, it is difficult to specify if the magnetic moments gradually rotate when the magnetic field increases (spin-flop transition), or if the magnetic moments go over directly from an antiferromagnetic alignment to a saturated paramagnetic alignment (metamagnetic transition). To solve this problem, the magnetization curve versus the magnetic field must be studied on a single crystal, as a function of the crystallographic directions.

6. Conclusion

The magnetic structure of $\text{Pb}_8\text{Fe}^{\text{II}}\text{Fe}_2^{\text{III}}\text{F}_{24}$ is solved and the results of the refinements appear to be consistent. The magnetic properties are in agreement with the magnetic structure. A spin-flop transition is evidenced for a magnetic field greater than 5000 Oe at 5 K. Nevertheless, to characterize more precisely this transition, it is necessary to study the properties of this fluoride (magnetization versus magnetic field, heat capacity) on a single crystal, for different temperatures below 21 K.

References

- [1] J. Renaudin, G. Férey, M. Zemirli, F. Varret, A. de Kozak, M. Drillon, NATO ASI series, Organic and inorganic low-dimensional crystalline materials, Plenum Publishing Corporation, 28B, 1987, p. 389.
- [2] A. Le Lirzin, J. Darriet, A. Tressaud, P. Hagenmuller, C.R. Acad. Sci. Paris 308 (II) (1989) 713.
- [3] E. Coronado, M. Drillon, A. Fuertes, D. Beltran, A. Mosset, J. Galy, J. Am. Chem. Soc. 108 (1986) 900.
- [4] V. Baron, B. Gillon, J. Sletten, C. Mathoniere, E. Codjovi, O. Kahn, Inorg. Chim. Acta 235 (1995) 69.
- [5] M. Drillon, E. Coronado, M. Balaiche, R.L. Carlin, J. Appl. Phys. 63 (8) (1988) 3551.
- [6] J. Aride, M. Taibi, S. Flandrois, M. Drillon, R.L. Carlin, Physics Letters A 152 (1,2) (1991) 114.
- [7] Q. Xu, J. Darriet, R. Georges, J. Magn. Magn. Mat. 73 (1988) 379.
- [8] Q. Xu, J. Darriet, J.L. Soubeyroux, R. Georges, J. Magn. Magn. Mat. 74 (1988) 219.
- [9] A. Pierrard, Thesis, 1998, Univ. P. et M. Curie, Paris, France.
- [10] A. Pierrard, A. de Kozak, P. Gredin, J. Renaudin, Z. anorg. allg. Chem. 621 (1995) 1053.
- [11] J. Rodriguez-Carvajal, FULLPROF: Rietveld, profile matching and

- integrated intensity refinement of X-ray and/or neutron data, 3.3 version (1997), Léon-Brillouin Laboratory, C. E. A.-Saclay, France.
- [12] J.C. Bernier, P. Poix, *L'actualité chimique*, February (1978) 7.
- [13] A. Desert, A. Bulou, M. Leblanc, J. Nouet, *J. Phys. Condens. Matter* 10 (1998) 9067.
- [14] P. Lacorre, J. Pannetier, J. Pebler, S. Nagel, D. Babel, A. de Kozak, M. Samouël, G. Férey, *J. Solid State Chem.* 101 (1992) 296.
- [15] O. Moze, E. Brück, K.H.J. Buschow, *J. Alloys Comp.* 281 (1998) 123.